

## Morpholino Monolayers: Preparation and Label-free DNA Analysis by Surface Hybridization

Napoleon Tercero,<sup>†,‡</sup> Kang Wang,<sup>†</sup> Ping Gong,<sup>‡</sup> and Rastislav Levicky<sup>\*,†</sup>

*Department of Chemical & Biological Engineering, Polytechnic Institute of New York University, Brooklyn, New York 11201, and Department of Chemical Engineering, Columbia University, New York, New York 10027*

Received December 24, 2008; E-mail: rlevicky@poly.edu

**Abstract:** Surface hybridization, a reaction in which nucleic acid molecules in solution react with nucleic acid partners immobilized on a surface, is widely practiced in life science research. In these applications the immobilized partner, or “probe”, is typically single-stranded DNA. Because DNA is strongly charged, high salt conditions are required to enable binding between analyte nucleic acids (“targets”) in solution and the DNA probes. High salt, however, compromises prospects for label-free monitoring or control of the hybridization reaction through surface electric fields; it also stabilizes secondary structure in target species that can interfere with probe–target recognition. In this work, initial steps toward addressing these challenges are taken by introducing morpholinos, a class of uncharged DNA analogues, for surface-hybridization applications. Monolayers of morpholino probes on gold supports can be fabricated with methods similar to those employed with DNA and are shown to hybridize efficiently and sequence-specifically with target strands. Hybridization-induced changes in the interfacial charge organization are analyzed with electrochemical methods and compared for morpholino and DNA probe monolayers. Molecular mechanisms connecting surface hybridization state to the interfacial capacitance are identified and interpreted through comparison to numerical Poisson–Boltzmann calculations. Interestingly, positive as well as negative capacitive responses (contrast inversion) to hybridization are possible, depending on surface populations of mobile ions as controlled by the applied potential. Quantitative comparison of surface capacitance with target coverage (targets/area) reveals a nearly linear relationship and demonstrates sensitivities (limits of quantification) in the picogram per square millimeter range.

### 1. Introduction

Surface hybridization, in which sequence-specific binding between polynucleic acid “probes” on a solid support and complementary “targets” from solution occurs at a solid–liquid interface, was introduced as a diagnostic method in the 1960s.<sup>1,2</sup> The technique continues to be widely exploited in modern DNA microarray and biosensor technologies for genotyping, transcriptome profiling, genetic identification, and related diagnostic applications.<sup>3</sup> When hybridization occurs at a surface, experiments show that the phenomenology of the reaction is more complex than in solution.<sup>4–17</sup> The crowded interfacial environment is characterized by nucleotide concentrations that approach

the molar range, and the resultant amplification of interactions between nucleotides can have a dramatic impact on physical behavior, manifesting, for example, in binding affinities orders of magnitude lower than those in solution.<sup>6,14,15,17,18</sup>

A consequence of molecular crowding is that a DNA probe layer presents a high,  $\sim 0.1$  mol L<sup>-1</sup>, concentration of immobilized negative charge. This charge density erects an electrostatic barrier to entry of like-charged would-be hybridization partners from solution. In order for hybridization to proceed, this barrier needs to be screened through the addition of salt such that the solution number density of mobile ions becomes

<sup>†</sup> Polytechnic Institute of New York University.

<sup>‡</sup> Columbia University.

- (1) Denhardt, D. T. *Biochem. Biophys. Res. Commun.* **1966**, *23*, 641–646.
- (2) Gillespie, D.; Spiegelman, S. *J. Mol. Biol.* **1965**, *12*, 829–842.
- (3) Müller, H.-J.; Röder, T. *Microarrays*; Elsevier Academic Press: Burlington, MA, 2006.
- (4) Watterson, J. H.; Piuino, P. A. E.; Wust, C. C.; Krull, U. J. *Langmuir* **2000**, *16*, 4984–4992.
- (5) Peterlinz, K. A.; Georgiadis, R. M.; Herne, T. M.; Tarlov, M. J. *J. Am. Chem. Soc.* **1997**, *119*, 3401–3402.
- (6) Peterson, A. W.; Wolf, L. K.; Georgiadis, R. M. *J. Am. Chem. Soc.* **2002**, *124*, 14601–14607.
- (7) Glazer, M.; Fidanza, J. A.; McGall, G. H.; Trulson, M. O.; Forman, J. E.; Suseno, A.; Frank, C. W. *Anal. Biochem.* **2006**, *358*, 225–238.
- (8) Yao, D. F.; Kim, J.; Yu, F.; Nielsen, P. E.; Sinner, E. K.; Knoll, W. *Biophys. J.* **2005**, *88*, 2745–2751.

- (9) Shchepinov, M. S.; Case-Green, S. C.; Southern, E. M. *Nucleic Acids Res.* **1997**, *25*, 1155–1161.
- (10) Wong, E. L. S.; Chow, E.; Gooding, J. J. *Langmuir* **2005**, *21*, 6957–6965.
- (11) Gong, P.; Lee, C.-Y.; Gamble, L. J.; Castner, D. G.; Grainger, D. W. *Anal. Chem.* **2006**, *78*, 3326–3334.
- (12) Gong, P.; Harbers, G. M.; Grainger, D. W. *Anal. Chem.* **2006**, *78*, 2342–2351.
- (13) Henry, M. R.; Stevens, P. W.; Sun, J.; Kelso, D. M. *Anal. Biochem.* **1999**, *276*, 204–214.
- (14) Nelson, B. P.; Grimsrud, T. E.; Liles, M. R.; Goodman, R. M.; Corn, R. M. *Anal. Chem.* **2001**, *73*, 1–7.
- (15) Okahata, Y.; Kawase, M.; Niikura, K.; Ohtake, F.; Furusawa, H.; Ebara, Y. *Anal. Chem.* **1998**, *70*, 1288–1296.
- (16) Ricci, F.; Lai, R. Y.; Heeger, A. J.; Plaxco, K. W.; Sumner, J. J. *Langmuir* **2007**, *23*, 6827–6834.
- (17) Gong, P.; Levicky, R. *Proc. Natl. Acad. Sci. U.S.A.* **2008**, *105*, 5301–5306.
- (18) Levicky, R.; Horgan, A. *Trends Biotechnol.* **2005**, *23*, 143–149.

comparable to that of the surface-bound DNA charge.<sup>17</sup> While this electrostatic screening benefits hybridization, it also suppresses electrostatic interactions between the probe layer and the underlying support that could be used to control or to monitor the surface hybridization state. As an alternative approach that avoids this drawback, electrostatic hindrance to surface hybridization can be tempered through the use of neutral (i.e., uncharged) probes, such as peptide nucleic acids (PNAs)<sup>19,20</sup> and morpholinos.<sup>21</sup> Moreover, because the probe layer starts from an uncharged state, binding of charged nucleic acid targets is expected to elicit stronger structural changes, thus enhancing prospects for analysis of the hybridization reaction through purely electrostatic means.

From the selection of neutral probes, the high binding affinity of PNAs provides strong mismatch discrimination<sup>19,22</sup> that is expected to be well suited to genotyping and to resequencing. Applications of PNAs have typically relied on 16mer or shorter sequences,<sup>23–26</sup> since longer strands, or ones containing long stretches of pyrimidines and purines, become increasingly challenging to prepare<sup>27–29</sup> and have greater potential for cross-reactivity with mismatched sequences. PNAs are thus expected to be less well suited to applications such as gene expression and pathogen detection which benefit from longer probe lengths, up to 70 nt,<sup>30,31</sup> to provide robust identification of a target's unique origin (i.e., a specific gene or biological entity). In such instances morpholinos, which place few constraints on sequence design or length, are expected to be advantageous. Morpholinos also mitigate some of the difficult physicochemical properties of neutral DNA analogues; for example, they are about 100-fold more soluble than comparable PNAs and their relatively stiff backbone reduces propensity toward self-aggregation.<sup>32</sup>

The principal goal of the present study was to fundamentally understand origins of electrostatic signatures of hybridization on charge-neutral morpholino layers, and to contrast this behavior with that of DNA probe films. The preparation of thiolate-anchored morpholino films on gold supports is described first, based on adaptation of “mixed monolayer” methods used for production of molecularly precise DNA films consisting of

the probe plus an alkanethiol surface-blocking agent.<sup>33–36</sup> The efficacy of the blocking agent to passivate against surface adsorption of the probe backbone is critical and was confirmed with infrared spectroscopy. Electrochemical methods were used to study hybridization between morpholino probes and DNA targets. Changes in layer organization, from probe–target binding, were related to the layer's capacitive (charging) response. The sensitivity and direction of the response, including observation of contrast inversion, were controllable by the surface potential,  $V_{DC}$ , at which the response was sampled. At the molecular level these relationships can be explained from the combined influence of  $V_{DC}$  and surface charge, stemming from hybridization of target strands, on the local populations of mobile ions, as further interpreted through Poisson–Boltzmann modeling. “Dual-color” redox labeling was used to simultaneously track surface populations of probe and target strands to derive a quantitative mapping between the capacitive response and the target occupancy. Viewed as a diagnostic tool for surface hybridization, these label-free capacitive measurements exhibit unoptimized sensitivities comparable to those of established methods such as surface plasmon resonance and quartz crystal microbalance techniques.

## 2. Materials and Methods

**2.1. Materials.** Morpholino oligomers, purified by precipitation, were purchased from Gene Tools LLC. HPLC purified DNA probes and targets were purchased from MWG Biotech. Table 1 lists the morpholino and DNA sequences, their abbreviations, and experimental purpose.

*N*-(2-Ferrocene-ethyl) maleimide (F2) was synthesized as described.<sup>17</sup> Synthesis of ferrocene monocarboxylic acid *N*-hydroxy-succinimide ester (FC1) was similar to published methods<sup>37</sup> and is detailed in the Supporting Information.

**2.2. Bioconjugation of Ferrocene Tags.** Electroactive tags F2 and FC1 were used to label target and probe molecules, respectively, to allow *in situ* determination of strand surface coverage. Amine-terminated probes PM1 and PD1 were labeled with FC1 at the 5' end (Figure S2, Supporting Information) by combining 0.3 mmol L<sup>-1</sup> probe in 0.5 mol L<sup>-1</sup> sodium carbonate buffer, pH 9.0, with a 150-fold excess of FC1 at room temperature for 16 h. Unreacted FC1 was removed on NAP-10 (GE Healthcare) and oligonucleotide purification cartridge (Applied Biosystems) prep columns, followed by reverse-phase HPLC (Beckman Coulter Gold 125; Clarity 3  $\mu$ m Oligo-RP column from Phenomenex). HPLC conditions for ferrocene-modified DNA probes were 50 °C, 0.5 mL min<sup>-1</sup>, and a linear gradient of 12 to 60% methanol in hexafluoroisopropanol/triethylamine buffer (HFIP–TEA; 100 mmol L<sup>-1</sup> HFIP, 4.5 mmol L<sup>-1</sup> TEA, pH 8.0) spread over 22 min. HPLC purification of morpholino–ferrocene conjugates proceeded identically but using a gradient of 12 to 100% methanol in HFIP–TEA over 20 min, followed by 5 min at 100% methanol. The dominant fraction of labeled material was collected and a second run performed to confirm purity. Conjugates were dried in a vacuum centrifuge (Vacufuge, Eppendorf) and stored dry at –14 °C until use. For experiments requiring labeled targets, additional TD1 and TD2 sequences (Table 1) were purchased that also included a 3' disulfide (–(CH<sub>2</sub>)<sub>3</sub>SS(CH<sub>2</sub>)<sub>3</sub>OH) end modification. Labeling of target oligonucleotides started with deprotection of the disulfide endgroup

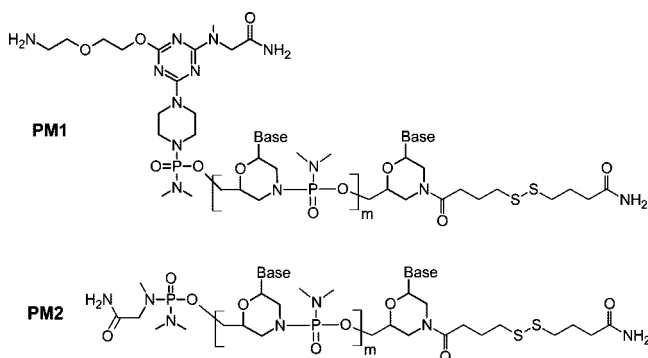
- (19) Egholm, M.; Buchardt, O.; Christensen, L.; Behrens, C.; Freler, S. M.; Driver, D. A.; Berg, R. H.; Kim, S. K.; Norden, B.; Nielsen, P. E. *Nature* **1993**, *365*, 566–568.
- (20) Tomac, S.; Sarkar, S.; Ratilainen, T.; Wittung, P.; Nielsen, P. E.; Nordén, B.; Gräslund, A. *J. Am. Chem. Soc.* **1996**, *118*, 5544–5552.
- (21) Summerton, J. In *Discoveries in Antisense Nucleic Acids*; Brakel, C., Ed.; Advances in Applied Biotechnology; Portfolio Publishing Co.: The Woodlands, TX, 1989; pp 71–80.
- (22) Ratilainen, T.; Holmn, A.; Tuite, E.; Nielsen, P. E.; Nordén, B. *Biochemistry* **2000**, *39*, 7781–7791.
- (23) Germini, A.; Mezzelani, A.; Lesignoli, F.; Corradini, R.; Marchelli, R.; Bordoni, R.; Consolandi, C.; De Bellis, G. *J. Agric. Food Chem.* **2004**, *52*, 4535–4540.
- (24) Weiler, J.; Gausepohl, H.; Hauser, N.; Jensen, O. N.; Hoheisel, J. D. *Nucleic Acids Res.* **1997**, *25*, 2792–2799.
- (25) Demidov, V. V.; Frank-Kamenetskii, M. D. *Trends Biochem. Sci.* **2004**, *29*, 62–71.
- (26) Brandt, O.; Feldner, J.; Stephan, A.; Schröder, M.; Schnölzer, M.; Arlinghaus, H. F.; Hoheisel, J. D.; Jacob, A. *Nucleic Acids Res.* **2003**, *31*, e119.
- (27) Altenbrunn, F.; Seitz, O. *Org. Biomol. Chem.* **2008**, *6*, 2493–2498.
- (28) Bergmann, F.; Bannwarth, W.; Tam, S. *Tetrahedron Lett.* **1995**, *36*, 6823–6826.
- (29) Gildea, B. D.; Casey, S.; MacNeill, J.; Perry-O'Keefe, H.; Sørensen, D.; Coull, J. M. *Tetrahedron Lett.* **1998**, *39*, 7255–7258.
- (30) Hughes, T. R.; et al. *Nat. Biotechnol.* **2001**, *19*, 342–347.
- (31) Bodrossy, L.; Sessitsch, A. *Curr. Opin. Microbiol.* **2004**, *7*, 245–254.
- (32) Summerton, J. E. *Lett. Pept. Sci.* **2004**, *10*, 215–236.
- (33) Herne, T. M.; Tarlov, M. J. *J. Am. Chem. Soc.* **1997**, *119*, 8916–8920.

- (34) Dandy, D. S.; Wu, P.; Grainger, D. W. *Proc. Natl. Acad. Sci. U.S.A.* **2007**, *104*, 8223–8228.
- (35) Baker, B. R.; Lai, R. Y.; Wood, M. S.; Doctor, E. H.; Heeger, A. J.; Plaxco, K. W. *J. Am. Chem. Soc.* **2006**, *128*, 3138–3139.
- (36) Levicky, R.; Herne, T. M.; Tarlov, M. J.; Satija, S. K. *J. Am. Chem. Soc.* **1998**, *120*, 9787–9792.
- (37) Takenaka, S.; Uto, Y.; Kondo, H.; Ihara, T.; Takagi, M. *Anal. Biochem.* **1994**, *218*, 436–443.

**Table 1.** Morpholino and DNA Sequences<sup>a</sup>

sequence	abbreviation	purpose
5' NH <sub>2</sub> -TTT TAA ATT CTG CAA GTG AT-CO(CH <sub>2</sub> ) <sub>3</sub> SS(CH <sub>2</sub> ) <sub>3</sub> CONH <sub>2</sub> 3'	PM1	morpholino retino- blastoma RB1 marker probe; used for hybridization studies
5' NH <sub>2</sub> -TTT TAA ATT CTG CAA GTG AT-(CH <sub>2</sub> ) <sub>3</sub> SS(CH <sub>2</sub> ) <sub>3</sub> OH 3'	PD1	DNA probe; same sequence as PM1
5' TTT TTT TCC TTC CTT TTT TT-CO(CH <sub>2</sub> ) <sub>3</sub> SS(CH <sub>2</sub> ) <sub>3</sub> CONH <sub>2</sub> 3'	PM2	morpholino probe; used for infrared reflection-absorption spectroscopy (IRRAS) studies
5' ATC ACT TGC AGA ATT TAA 3'	TD1	DNA target; complementary to PM1 and PD1
5' AAA AAA AGG AAG GAA AAA 3'	TD2	DNA target; noncomplementary hybridization control

<sup>a</sup> The morpholino PM1 and PM2 molecular structures are ( $m = 19$ )



with dithiothreitol (DTT) to liberate the sulfhydryl moiety, in 10 mmol L<sup>-1</sup> DTT, 10 mmol L<sup>-1</sup> TRIS, 1 mmol L<sup>-1</sup> EDTA, pH 8.0, for 2 h. Excess DTT was removed on a NAP-10 column, followed by reacting the ~25 μmol L<sup>-1</sup> target solution with 30-fold excess of F2 (Figure S2, Supporting Information) in 150 mmol L<sup>-1</sup> potassium phosphate buffer, pH 8.0, overnight. Final purification, collection, drying, and storage procedures were as for DNA probes.

**2.3. Preparation of Probe Monolayers.** Samples for electrochemical measurements were prepared on 1.6 mm diameter polycrystalline gold disk electrodes. The electrodes were first cleaned by mechanical polishing with 1 μm diamond suspension, rinsing with methanol and deionized (18.2 MΩ cm) water, and finally by potentiodynamic cycling in 0.5 mol L<sup>-1</sup> H<sub>2</sub>SO<sub>4</sub> for 60 cycles from 0.24 to 1.54 V (vs Ag/AgCl/3 mol L<sup>-1</sup> NaCl reference) at 0.1 V s<sup>-1</sup>. The electrodes were again rinsed with deionized water, and without drying, the roughness factor  $r$  ( $r = \text{actual area/ geometric area}$ ) was determined from double-layer capacitance.<sup>38,39</sup> Values of  $r$  ranged from 1.4 to 1.6. After a final rinse with deionized water, the still-wet electrodes were covered by probe deposition solution.

Probe solutions were pipetted directly onto cleaned supports. Probes were suspended at 0.25 μmol L<sup>-1</sup> probe in deionized water (morpholino probes) or in 1 mol L<sup>-1</sup> MgCl<sub>2</sub> (DNA probes). Following immobilization of the probes, samples were rinsed with deionized water and then blocked in 1 mmol L<sup>-1</sup> mercaptopropanol (MCP; Sigma-Aldrich 95% purity) in water for 90 min for DNA layers, or for 150 min for morpholino layers. The longer blocking times for morpholinos improved reproducibility of baselines in cyclic voltammetry experiments. The samples were rinsed again

and placed into target-free hybridization buffer (see below). All transfer steps were accomplished wet to minimize chances for adsorption of atmospheric contaminants.

Samples for infrared reflection-absorption spectroscopy (IRRAS) were prepared on standard-size, float glass microscope slides coated with 5 nm of titanium and 100 nm of gold (EMF Corp., Ithaca, NY). The slides were cleaned for 10 min in 120 °C “piranha” solution consisting of 7:3 mixture of concentrated sulfuric acid and 30% hydrogen peroxide solution in water (**Caution:** *Piranha solution is highly oxidizing and must not be stored in tightly capped containers on account of gas evolution.*) Following a rinse with deionized water, the still-wet slides were covered with probe deposition solution. Conditions were as for preparation of electrochemical samples except that, in addition, slides were prepared also without the final MCP blocking step. After drying with a nitrogen stream, samples were used immediately for IRRAS measurements.

**2.4. IRRAS Measurements.** IRRAS spectroscopy was performed on a Perkin-Elmer Spectrum 100 spectrometer equipped with an 80° specular reflectance accessory (PIKE Technologies). Spectra were collected from 900 to 4000 cm<sup>-1</sup> at 4 cm<sup>-1</sup> resolution, with software correction for the presence of water vapor bands. Cleaned, but otherwise unmodified, gold-coated slides served as background.

**2.5. Electrochemical Characterization.** Electrochemical measurements were performed on a CHI660C workstation (CH Instruments) with a three-electrode cell comprised of the modified Au working electrode, a platinum wire counter electrode, and an Ag/AgCl/3 mol L<sup>-1</sup> NaCl reference electrode (Bioanalytical Systems; 0.209 V vs NHE at 25 °C). All potentials are reported relative to this reference. A glass sleeve salt bridge was used to guard against leakage of NaCl from the reference electrode’s reservoir into the electrolyte. The electrolyte, which also served as the hybridization buffer, was 0.2 mol L<sup>-1</sup> sodium phosphate buffer, pH 7.0. A fixed target concentration of 25 nmol L<sup>-1</sup> and probe coverages of about 5 × 10<sup>12</sup> probes cm<sup>-2</sup> were used. When data were not being collected, the electrochemical cell was kept off.

Cyclic voltammetry (CV) measurements to determine the instantaneous coverage of ferrocene-labeled strands used a scan rate of 20 V s<sup>-1</sup> from 0 to 0.6 V or to 0.65 V, requiring approximately 0.07 s per cycle. Probe and target surface coverages,  $S_P$  and  $S_T$ , were calculated from the charge  $Q$  associated with oxidation of their ferrocene tags:

$$S_P = Q_{\text{FC1}}/(eA_g r) \quad S_T = Q_{\text{F2}}/(eA_g r) \quad (1)$$

where  $e = 1.60 \times 10^{-19}$  C is the elementary charge,  $A_g$  is the geometric area occupied by the probe layer, and  $r$  is the measured roughness factor.  $Q_{\text{FC1}}$  and  $Q_{\text{F2}}$  are total charges from the oxidation  $\text{FC1} \rightarrow \text{FC1}^+ + e^-$  and  $\text{F2} \rightarrow \text{F2}^+ + e^-$ , respectively, corresponding to integration of the blue and green areas in Figure 1 after converting the potential axis to time. Each probe and target possesses one ferrocene tag. The “T” peak near 0.25 V represents increased current due to oxidation of F2 and confirms the presence of surface-bound target molecules. The probe FC1 signal, labeled “P”, is observed near 0.45 V. On the reverse scan the tags are reset back to the neutral ferrocene state. The figure also shows fits to the data from which  $Q_{\text{FC1}}$  and  $Q_{\text{F2}}$  were determined. Fits were calculated by an automated computer routine described in the Supporting Information.

In AC impedance (ACI) measurements, (1) a steady bias,  $V_{\text{DC}}$ , is imposed to set up the surface environment (e.g., distribution of mobile ions), and (2) the charge-flow (current) response of this environment to perturbations in potential is sampled using a weak sinusoidal read-out function added to  $V_{\text{DC}}$ . Under the experimental conditions used, the response consisted only of charging currents, with the electrochemical cell behaving as a series combination of a resistance,  $R$ , representing the electrolyte, and a differential capacitance per area,  $C_d$ , representing the probe-modified working electrode.  $C_d$  characterizes the surface organization of the probe

(38) Oesch, U.; Janata, J. *Electrochim. Acta* **1983**, *28*, 1237–1246.

(39) Shen, G.; Tercero, N.; Gaspar, M. A.; Varughese, B.; Shepard, K.; Levicky, R. *J. Am. Chem. Soc.* **2006**, *128*, 8427–8433.

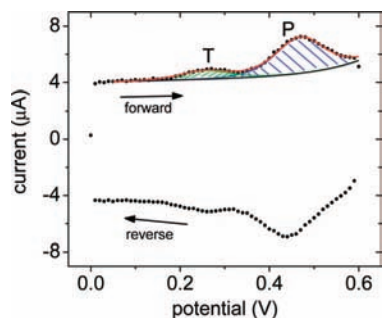


**Figure 1.** Cyclic voltammetry. Points are experimental data. The CV scan starts from 0 V, moves along the forward trace to 0.6 V, and returns to 0 V along the reverse trace. The “T” and “P” peaks are from oxidation of target F2 and probe FC1 tags. The curves are computer-generated fits used to calculate  $Q_{FC1}$  and  $Q_{F2}$  (Supporting Information). Black line, baseline current  $I_B$  (eq S2, Supporting Information); green line, current  $I_{T,F2}$  from target tags (eq S3); blue line, current  $I_{T,FC1}$  from probe tags (eq S3); red line, total current  $I_{tot} = I_B + I_{T,F2} + I_{T,FC1}$ .

layer and, for a series RC arrangement, is calculated from the measured out-of-phase impedance  $Z''$  using  $|Z''| = 1/(2\pi f A_g r C_d)$ .  $f$  is the read-out frequency.  $Z''$  is related to experimental quantities via  $Z'' = -V_{ac} I_{op}/(I_{ip}^2 + I_{op}^2)$ , with  $V_{ac}$  the magnitude of the imposed read-out function and  $I_{ip}$  and  $I_{op}$  the magnitudes of the measured in-phase and out-of-phase current components, respectively. A useful interpretation of  $C_d$  is as a metric of the near-surface screening of electric fields: more effective screening correlates with higher capacitance because greater charge  $d\sigma_0$  must be placed on the electrode to achieve a potential increment  $dV$  (see eq 2 below). Screening can be provided by polarization of the surface environment, as governed by the local dielectric properties, and/or by redistribution of mobile ionic charge.

An ACI measurement consisted of stepping the surface bias  $V_{DC}$  from 0.25 to  $-0.2$  V in 0.025 V steps and back, with  $C_d$  determined at each step. A full  $C_d$ -loop took 1 min and was performed once every 5 min during the course of hybridization. A read-out frequency  $f = 5435$  Hz and ac potential magnitude of 5 mV rms were used. This frequency corresponded to a phase angle of  $45$ – $50^\circ$  and was sufficiently low to avoid secondary capacitive charging observed in the presence of the salt bridge at high frequencies, yet high enough to minimize contributions from spurious interfacial charge transfer that become more prominent at low frequencies.

**2.6. Theoretical Calculation of  $C_d$ .** Theoretical predictions of the behavior of  $C_d$  were used to guide interpretation of observed experimental trends.  $C_d$  is defined by the derivative of the surface charge per area of the electrode,  $\sigma_0$ , with respect to the electrode potential  $V$ :

$$C_d = \frac{d\sigma_0}{dV} \quad (2)$$

$$\sigma_0 = -\epsilon\epsilon_0 \left( \frac{dV}{dx} \right)_{0 \leftarrow x} \quad (3)$$

where eq 3 follows from Gauss's law. Here  $\epsilon$  is the material dielectric constant (relative static permittivity),  $\epsilon_0$  is the permittivity of vacuum, and  $x$  is the perpendicular distance from the electrode surface.  $V(x)$  was calculated by numerical integration of the Poisson–Boltzmann equation,

$$\frac{d^2V}{dx^2} = -\frac{\rho(x)}{\epsilon(x)\epsilon_0} \quad (4)$$

$$\rho(x) = z_1 e c_1(x) + \sum_j z_j e c_{j\infty} \exp(-z_j e V(x)/kT) \exp(-\beta_j(x)) \quad (5)$$

$\rho(x)$  is the concentration of charge at  $x$ ,  $e$  is the unit charge ( $1.60 \times 10^{-19}$  C),  $z_1$  and  $c_1$  are the valence and concentration of immobile charged sites (e.g.,  $c_1$  might represent concentration of DNA backbone phosphate residues),  $T$  is absolute temperature,  $k$  is the Boltzmann constant, and  $z_j$ ,  $c_{j\infty}$ , and  $\beta_j$  are the valence, solution concentration, and partitioning penalty of species  $j$ , respectively, where  $j$  ranges over all ions free to partition between solution and the probe layer. For example, if in the probe layer  $\beta_{Na^+} = 1$ , then there is a  $1kT$  penalty to transport a  $Na^+$  cation from solution to the layer (e.g., from changes in solvation interactions) in addition to the  $eV$  term.

Equations 4 and 5 were solved for  $V(x)$  by modeling the MCP/probe film/electrolyte structure as a multilayer inside of which each layer  $k$ , of width  $t_k$ , was specified by constant values of  $\epsilon_k$ ,  $c_{1k}$ , and  $\beta_k$ . Runge–Kutta–Verner fifth- and sixth-order methods were used to integrate eq 4, expressed as two ordinary differential equations  $dy_1/dx = -\rho_k/(\epsilon_k\epsilon_0)$  and  $dy_2/dx = y_1$ , where  $y_2 = V(x)$ . The integration was performed from the probe layer/electrolyte interface at  $x_B = \sum_k t_k$  to the electrode surface at  $x = 0$ , with continuity of the potential  $V(x)$  and electric displacement  $\epsilon dV/dx$  at boundaries between layers. The two required initial conditions were (1) a specified value for  $V(x_B)$  and (2) the corresponding potential gradient  $dV/dx$  at  $x = x_B$ . The gradient can be calculated by integrating eq 4 analytically once; if  $x_1$  and  $x_2$  are two positions within layer  $k$ , then

$$\left( \frac{dV}{dx} \right)_{x_2} = \left( \left( \frac{dV}{dx} \right)_{x_1}^2 - \frac{2eN_A}{\epsilon_k\epsilon_0} \left[ z_{1k} c_{1k} (V_2 - V_1) + \frac{kT}{e} \sum_j c_j \exp(-z_j e V_2/kT - \beta_{jk}) \{ \exp(z_j e (V_2 - V_1)/kT - 1) \} \right] \right)^{1/2} \quad (6)$$

For the semi-infinite electrolyte with  $x_2 = x_B$ ,  $x_1 = \infty$ ,  $c_1 = 0$ , and  $\beta_j = 0$ , and with  $dV/dx$  and  $V$  going to 0 as  $x \rightarrow \infty$ , eq 6 simplifies to

$$\left( \frac{dV}{dx} \right)_{x_B} = \left( -\frac{2kTN_A}{\epsilon\epsilon_0} \sum_j c_j \{ 1 - \exp(-z_j e V(x_B)/kT) \} \right)^{1/2} \quad (7)$$

which served as the second initial condition.  $C_d$  was obtained from the calculated  $V(x)$  by numerical differentiation, according to eqs 2 and 3.

The electrolyte was modeled as containing sodium cations and three types of phosphate anions with relative concentrations governed by acid–base equilibria:  $H_2PO_4^-$ ,  $HPO_4^{2-}$ , and  $PO_4^{3-}$ . For the experimental  $0.2 \text{ mol L}^{-1}$  phosphate buffer, pH 7.0, the concentrations used are  $0.315 \text{ mol L}^{-1} Na^+$ ,  $0.0846 \text{ mol L}^{-1} H_2PO_4^-$ ,  $0.115 \text{ mol L}^{-1} HPO_4^{2-}$ , and  $5.54 \times 10^{-7} \text{ mol L}^{-1} PO_4^{3-}$ . The electrolyte dielectric constant was taken to be 80, and the temperature was 295 K.

### 3. Results and Discussion

**3.1. IRRAS Studies of MCP Passivation.** Direct contact of probes with the solid support can be detrimental to hybridization activity; for example, single-stranded DNA probes are known to adsorb to gold through base–surface interactions<sup>40,41</sup> that result in surface-bound conformations with poor hybridization

(40) Kimura-Suda, H.; Petrovykh, D. Y.; Tarlov, M. J.; Whitman, L. J. *J. Am. Chem. Soc.* **2003**, *125*, 9014–9015.

(41) Wolf, L. K.; Gao, Y.; Georgiadis, R. M. *Langmuir* **2004**, *20*, 3357–3361.

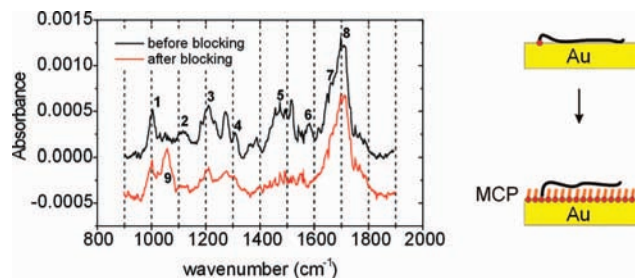


**Figure 2.** IRRAS spectra before (black line) and after (red line) blocking of a PM2 monolayer with mercaptopropanol (MCP). Assignments for numbered peaks are provided in Table 2. Peak 6 is diagnostic of contact between thymine bases and the Au support.

**Table 2.** IRRAS Spectral Assignments for Morpholino Monolayers

peak <sup>a</sup>	position (cm <sup>-1</sup> )	primary attribution	ref
1	1000	P—O—C asymmetric stretch	44
2	1120	C—O—C asymmetric stretch	44
3	1210	P=O stretch	44
4	1310	phosphoramidate (CH <sub>3</sub> ) <sub>2</sub> N <sup>-</sup> vibration	45
5	1420–1520	various bands (thymine, phosphoramidate)	42, 45
6	1580	C=O stretch of chemisorbed thymine	42
7	1670	C4=O stretch of thymine	42
8	1705	C2=O stretch of thymine	42
9	1060	C—OH stretch of mercaptopropanol	44

<sup>a</sup> See Figure 2 for peak labeling.

activity.<sup>11,33,36</sup> Hybridization activity can be restored by treatment, or passivation, of the surface with alkanethiols such as mercaptohexanol or mercaptopropanol (MCP) with a hydrophilic surface chemistry to which the probes do not strongly adsorb. These displacer molecules assemble into a monolayer coating that lifts the probe backbone off the support, leaving the strands attached through their thiolate bond only, in an end-tethered geometry favorable to hybridization.

Morpholino probes, through their bases, were similarly expected to exhibit an affinity for gold, motivating examination of whether MCP is able to successfully displace these interactions. The thymine-rich probe PM2 was selected for these experiments because thymine–gold interactions yield an IR marker band in the region 1580–1600 cm<sup>-1</sup><sup>42,43</sup> attributed to C=O stretches of chemisorbed thymine.<sup>42</sup> A successful passivation of the surface with MCP, in which the probe backbone is displaced from direct contact with the support, should be accompanied by a disappearance of this marker band.

Figure 2 compares IRRAS spectra of a PM2 monolayer before and after MCP blocking. The assignments for the dominant spectral bands are given in Table 2. The disappearance of the marker band, corresponding to peak 6, after MCP passivation indicates that displacement of adsorptive contacts between thymine bases and the support was successful. In parallel, the appearance of the C—OH stretch at 1060 cm<sup>-1</sup> (peak 9) confirms the surface presence of MCP.

**3.2. Charge Organization of Hybridized Morpholino Monolayers.** A specific state of surface hybridization defines a unique combination of immobilized and mobile ion concentrations at the surface. The response of this environment to an applied

potential can be used to characterize the state of hybridization and, in principle, provides for a convenient, label-free approach to diagnostics. However, significant challenges arise in quantitatively relating a label-free electrochemical response (e.g., surface capacitance, surface potential, field-effect transduction) with molecular coverage of analyte. The underlying relationships between surface organization and the measured response are obscure and at times counter-intuitive; for example, both decreases<sup>46–50</sup> and increases<sup>51–53</sup> in surface capacitance due to hybridization have been reported, illustrating that even the direction of change can be unpredictable. Similarly, orders of magnitude disparities exist in estimated sensitivities of field-effect transduction, despite similar mechanisms of contrast.<sup>54</sup>

In this section, the aim is to fundamentally understand the physical changes induced in charge organization of morpholino films undergoing hybridization, and to compare these to the observations when DNA probes are used. Optimization of morpholino assays, which perform best at low salt concentrations where DNA probes do not function, will be reported separately. At the buffer strength (0.2 mol L<sup>-1</sup> sodium phosphate, pH 7.0) used for the present experiments, both probe types hybridize well. In the experiments that will be described, the surface state was characterized at a point in time during the course of hybridization as a function of applied surface potential,  $V_{DC}$ , through the change in surface capacitance,  $\Delta C_d(V_{DC})$ , brought on by probe–target binding. In turn,  $\Delta C_d$  can be interpreted in terms of the near-surface ionic concentrations and dielectric strength. All of the experiments of this section used unlabeled targets in order to extend the positive limit on  $V_{DC}$  up to 0.25 V without interference from tag electroactivity in the determination of  $C_d$ , at the cost of foregoing quantification of target coverage (quantitative comparison of target coverage with  $\Delta C_d$  is postponed to section 3.3). Control experiments showed that (1) target coverage was not significantly perturbed by changes in surface potential during  $C_d$  measurements (Supporting Information, Figure S3) and (2) hybridization of morpholino films was sequence-specific, with binding of noncomplementary TD2 targets below detection (Supporting Information, Figure S4).

Figure 3 compares the evolution of  $\Delta C_d$  for morpholino (Figure 3A) and DNA (Figure 3B) probe films in the presence of target molecules. The insets show raw data in the form of traces of  $C_d$  vs time. Prior to addition of complementary target TD1 at time  $t = 0$ , only a featureless increase in the baseline, on the order of 1% per hour, was observed in the raw data. The source of this increase is not known with certainty but is suspected to reflect gradual loss of MCP. Empirically, the shape

- (42) Haiss, W.; Roelfs, B.; Port, S. N.; Bunge, E.; Baumgärtel, H.; Nichols, R. J. *J. Electroanal. Chem.* **1998**, *454*, 107–113.  
 (43) Petrovykh, D. Y.; Kimura-Suda, H.; Whitman, L. J.; Tarlov, M. J. *J. Am. Chem. Soc.* **2003**, *125*, 5219–5226.  
 (44) Socrates, G. *Infrared Characteristic Group Frequencies*, 2nd ed.; John Wiley & Sons Inc.: New York, 1994.  
 (45) Harvey, R. B.; Mayhood, J. E. *Can. J. Chem.* **1955**, *33*, 1552–1565.

- (46) Berggren, C.; Stålhandske, P.; Brundell, J.; Johansson, G. *Electroanalysis* **1999**, *11*, 156–160.  
 (47) Stagni, C.; Guiducci, C.; Benini, L.; Ricco, B.; Carrara, S.; Samori, B.; Paulus, C.; Schienle, M.; Augustyniak, M.; Thewes, R. *IEEE J. Solid-State Circuits* **2006**, *41*, 2956–2964.  
 (48) Shin, J. K.; Kim, D. S.; Park, H. J.; Lim, G. *Electroanalysis* **2004**, *16*, 1912–1918.  
 (49) Berggren, C.; Bjarnason, B.; Johansson, G. *Electroanalysis* **2001**, *13*, 173–180.  
 (50) Guiducci, C.; Stagni, C.; Fischetti, A.; Mastromatteo, U.; Benini, L.; Ricco, B. *IEEE Sensors J.* **2006**, *6*, 1084–1093.  
 (51) Mearns, F. J.; Wong, E. L. S.; Short, K.; Hibbert, D. B.; Gooding, J. J. *Electroanalysis* **2006**, *18*, 1971–1981.  
 (52) Yang, W. S.; Butler, J. E.; Russell, J. N.; Hamers, R. J. *Langmuir* **2004**, *20*, 6778–6784.  
 (53) Kafka, J.; Panke, O.; Abendroth, B.; Lisdat, F. *Electrochim. Acta* **2008**, *53*, 7467–7474.  
 (54) Poghosian, A.; Cherstvy, A.; Ingerbrandt, S.; Offenhäuser, A.; Schöning, M. J. *Sens. Actuators, B* **2005**, *111–112*, 470–480.

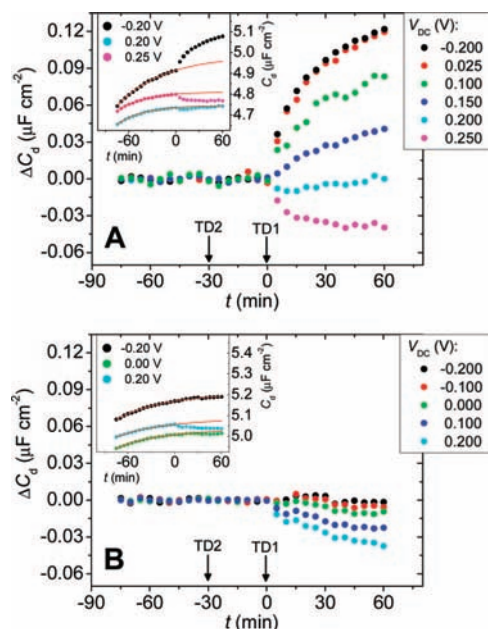


**Figure 3.** (A) Main panel: Change in capacitance  $\Delta C_d$  for morpholino layers undergoing hybridization as a function of measurement bias  $V_{DC}$ . Arrows indicate addition of noncomplementary TD2 and complementary TD1 targets. Inset: Examples of raw  $C_d$  vs time data (points) and fitted baselines  $f_B$  (red solid lines) at three settings of  $V_{DC}$ .  $\Delta C_d$  was calculated as the difference between  $C_d$  and the baseline. Conditions:  $4.9 \times 10^{12}$  probes  $\text{cm}^{-2}$ ,  $25 \text{ nmol L}^{-1}$  target,  $0.2 \text{ mol L}^{-1}$  sodium phosphate buffer, pH 7.0. (B) Same as (A) but for DNA probe layers at  $5.1 \times 10^{12}$  probes  $\text{cm}^{-2}$  and otherwise identical conditions.

of the baseline could be represented by a first-order process; that is, the baseline function  $f_B$  was modeled as  $f_B = A_1 - A_2 \exp(-A_3 t)$ , with  $A_1$ ,  $A_2$ , and  $A_3$  determined from a least-squares fit to data prior to hybridization,  $-75 < t < 0 \text{ min}$  (see insets to Figure 3).  $\Delta C_d$ , attributed to binding of target molecules, follows from  $\Delta C_d = C_d - f_B$ . For each run, probe layers were measured first under target-free buffer, next under  $25 \text{ nmol L}^{-1}$  non-complementary TD2 target for 30 min ( $-30 < t < 0 \text{ min}$ ), and finally under a TD1:TD2 mixture with each target present at  $25 \text{ nmol L}^{-1}$ . Addition of noncomplementary TD2 at  $t = -30 \text{ min}$  did not produce a resolved response at any of the potentials, whereas addition of the complementary TD1 target at  $t = 0 \text{ min}$  immediately led to a change in  $\Delta C_d$ .

Strikingly, as shown in the main panel of Figure 3A, the response of morpholino films to hybridization was tunable, with a change in sign (contrast inversion) from positive to negative as  $V_{DC}$  increased past  $0.2 \text{ V}$ . Moreover, in the range from  $-0.2$  to  $0.025 \text{ V}$ , the response was nearly independent of  $V_{DC}$ , making this range attractive for diagnostic applications. Above  $0.025 \text{ V}$ ,  $\Delta C_d$  started to decrease with  $V_{DC}$  and became negative beyond the contrast inversion point at  $0.2 \text{ V}$ . In comparison, hybridization of DNA targets to DNA probes produced  $\Delta C_d \approx 0$  when measured at negative biases, below  $-0.1 \text{ V}$ . As  $V_{DC}$  increased, contrast improved and an increasingly negative ( $\Delta C_d < 0$ ) response to hybridization was observed.

The data in Figure 3 show that, depending on  $V_{DC}$  and probe type, binding of target molecules can manifest as an increase, a decrease, or a null response. Understanding the origins of this diversity of trends provides insight into the physical changes that accompany surface hybridization. In Figure 4, the data are replotted to show the full dependence of  $C_d$  on  $V_{DC}$  at selected time points, for morpholino (Figure 4A) and DNA (Figure 4B) probe layers. Between  $t = -75$  (black points) and  $0 \text{ min}$  (black

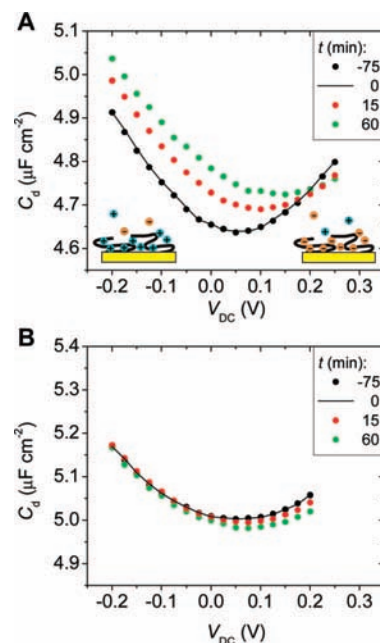


**Figure 4.**  $C_d(V_{DC})$  traces as a function of time for (A) morpholino and (B) DNA probe films.  $t = 0$  (black line) corresponds to introduction of complementary TD1 target and onset of hybridization. Shift in  $C_d$  due to baseline drift was corrected relative to  $t = 0$  by plotting  $C_d(t) = C_{d,\text{raw}}(t) - (f_B(t) - f_B(0))$ , where  $f_B(t) - f_B(0)$  is the change in baseline between  $t$  and  $0 \text{ min}$ , and  $C_{d,\text{raw}}(t)$  is the unprocessed data.

trace), the probe films were kept under buffer and noncomplementary TD2 target, with little, if any, change taking place. Introduction of complementary TD1 target at  $t = 0$  produced horizontal and vertical displacements of the  $C_d(V_{DC})$  trace. As illustrated by the cartoons in Figure 4A, the ubiquitous increase in  $C_d$  at the extremes of  $V_{DC}$  is attributed to potential-driven accumulation of solution ions near the surface: phosphate anions at more positive potentials and sodium cations when  $V_{DC}$  is swept negatively. The elevation in surface concentration of mobile ions provides for more efficient ionic screening, and hence higher capacitance.<sup>55</sup>

The displacements of the  $C_d(V_{DC})$  traces in Figure 4 were interpreted with the help of the Poisson–Boltzmann (PB) model, described by eqs 2–7. The MCP layer was modeled using a width  $t_{\text{MCP}} = 0.67 \text{ nm}$ ,<sup>56</sup> a dielectric constant  $\epsilon_{\text{MCP}} = 4.4$ , and  $\beta = 1000$  for all solution ions. These settings reproduced the experimental capacitance of about  $5.6 \mu\text{F cm}^{-2}$  for a pure MCP monolayer. Setting the partitioning penalty  $\beta$  to 1000 effectively renders the MCP layer impermeable to ions. The description of the morpholino layer proved more complex. One expectation is that unhybridized probes are in a collapsed, desolvated state. The principal reason for this suspicion is that the surface concentration of  $\sim 0.1\text{--}1 \text{ mol L}^{-1}$  significantly exceeds the bulk solubility of  $\sim 1 \text{ mmol L}^{-1}$ ,<sup>57</sup> implying that the probes exist as a precipitated film. As a first approximation, therefore, the layer thickness  $t_p$  was set to the collapsed “dry” value of  $0.52 \text{ nm}$ ,

(55) Backbone charges on DNA strands can also contribute to ionic screening; however, this contribution is expected to be relatively minor due to constraints imposed by their connectivity and the higher mass (lower mobility) of the polymer backbone.

(56)  $t_{\text{MCP}}$  was estimated from mass density of MCP,  $d = 1.07 \text{ g cm}^{-3}$ , molar mass of MCP,  $m = 92 \text{ g mol}^{-1}$ , and surface coverage of alkanethiol monolayers on gold,  $\sigma = 4.7 \times 10^{14} \text{ molecules cm}^{-2}$  (Strong, L.; Whitesides, G. M. *Langmuir* **1988**, *4*, 546–558).  $t_{\text{MCP}} = \sigma m / (d N_A)$ .

(57) Moulton, J., Gene Tools, personal communication.

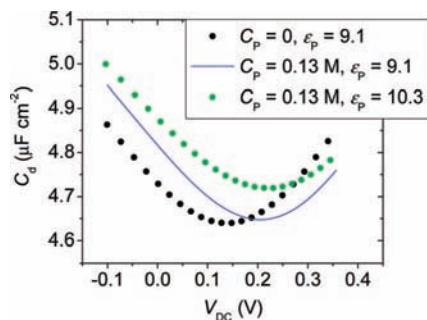


**Figure 5.** PB theory calculations, illustrating the effect of (1) an increase in immobilized negative charge  $C_p$  of the probe layer from 0 (black points) to  $0.13 \text{ mol L}^{-1}$  (blue line), and (2) an increase in dielectric constant  $\epsilon_p$  of the probe layer from 9.1 (blue line) to 10.3 (green points). The shape of the curve traced out by the black points corresponds, approximately, to  $t = 0$  data in Figure 4A, while the green trace can be compared to the  $t = 60$  min data. MCP layer parameters:  $t_{\text{MCP}} = 0.67 \text{ nm}$ ,  $\epsilon_{\text{MCP}} = 4.4$ ,  $\beta_{j,\text{MCP}} = 1000$  for all ions. Morpholino probe layer parameters:  $t_p = 0.52 \text{ nm}$ ,  $\beta_{\text{Na}^+,\text{P}} = 0$ ,  $\beta_{\text{H}_2\text{PO}_4^-\text{P}} = 1.8$ ,  $\beta_{\text{HPO}_4^{2-}\text{P}} = 1000$ ,  $\beta_{\text{PO}_4^{3-}\text{P}} = 1000$ . Electrolyte parameters:  $T = 295 \text{ K}$ ,  $0.2 \text{ mol L}^{-1}$ , phosphate buffer, pH 7.0.

derived from the measured probe coverage and a volume of  $0.53 \text{ nm}^3$  per nucleotide.<sup>58</sup>

In order to capture the experimental upturn in  $C_d$  at positive and negative biases (Figure 4A), it was necessary to allow sodium ( $\text{Na}^+$ ) and monovalent phosphate ( $\text{H}_2\text{PO}_4^-$ ) ions to partition into the probe film under the influence of  $V_{\text{DC}}$ . This condition was met by keeping the partitioning penalty  $\beta$  small for these ions (see Figure 5 caption). However, partitioning of divalent phosphate ( $\text{HPO}_4^{2-}$ ) led to an overly exaggerated upturn at positive  $V_{\text{DC}}$ ; thus, only monovalent phosphate was assumed to penetrate.<sup>59</sup> Finally, it is important to note that experiments express  $V_{\text{DC}}$  relative to a reference electrode, with an unknown absolute potential, whereas calculations express  $V_{\text{DC}}$  relative to solution. This leads to an offset in  $V_{\text{DC}}$  between calculated and experimental curves.<sup>60</sup>

Figure 5 shows that two simple adjustments in model parameters were able to qualitatively reproduce experimentally observed changes in  $C_d$  due to hybridization. The first type of adjustment consists of addition of immobile charge sites to the morpholino layer ( $c_1$  term in eq 5), the predominant outcome of which is a horizontal shift of the  $C_d(V_{\text{DC}})$  curve parallel to the potential axis. In Figure 5 this is illustrated by the black and blue traces representing, respectively, a neutral film and a layer with  $0.13 \text{ mol L}^{-1}$  concentration of immobile negative charge.<sup>61</sup> The horizontal shift arises because of an altered permselectivity of the film. The effect can be recast in hybridization terms as follows. Binding of targets introduces immobile, negatively charged sites to the probe layer. The presence of these sites depletes anions and accumulates cations

in the film, and alters the value of  $C_d$ . In order to restore  $C_d$  and the cation-to-anion balance at the surface to their prehybridization values, a more positive  $V_{\text{DC}}$  must be applied to compensate for the effect of the negatively charged sites. This positive offset in  $V_{\text{DC}}$  manifests as a translation of the entire  $C_d(V_{\text{DC}})$  curve toward positive potentials.

The above explanation and the PB model present a simplified description in that the charge of hybridized targets was assumed to be strictly immobile. This approximation is partly justified by the observation that, at the high frequency (5435 Hz) used for measurement, surface-tethered DNA oligonucleotide chains do not respond significantly to oscillating surface fields;<sup>62</sup> thus, the main contribution to  $C_d$  is expected to be from movement of small ions whose mobility is not impaired by backbone connectivity, or the large mass-to-charge ratio of DNA.

The second type of adjustment illustrated in Figure 5 is a change in the dielectric constant profile. In general, such a change could result from variation in composition, thickness, homogeneity, or other structural rearrangement of the probe layer brought on by hybridization. The local dielectric constant represents capacity of the surface environment to screen electric fields through polarization: higher values correspond to more effective screening, allowing greater surface charge to build up in response to an increment in potential, and increasing  $C_d$  (eq 2). A change in dielectric constant thus raises or lowers  $C_d$ ,<sup>63</sup> causing a vertical displacement of the  $C_d(V_{\text{DC}})$  curve. This is illustrated in Figure 5, where an upward displacement was produced by increasing the dielectric constant of the probe film from 9.1 (blue curve) to 10.3 (green trace).

For morpholino films, the impact of hybridization on the  $C_d(V_{\text{DC}})$  curve can be summarized as a rightward and an upward translation (Figure 4A). The rightward displacement signifies a change in permselectivity that favors cations and expels anions; as discussed above, this outcome is expected from hybridization of negatively charged targets. The upward displacement indicates improved dielectric screening. These dielectric changes are expected to reflect various effects, difficult if not impossible to disentangle. For example, hybridization may improve solvent compatibility of the probe layer, elevating the local dielectric constant through increased water content, and concomitantly leave a thinner underlayer of unhybridized, collapsed probes on the surface. It is the cumulative effect of such changes that would be reflected in the observed, upward displacement in  $C_d$ .

Hybridization to DNA probes resulted in a rightward displacement of the  $C_d(V_{\text{DC}})$  curve (Figure 4B), indicating that, also in this case, binding of target molecules shifted the cation-to-anion balance in favor of cations. The qualitative impact of hybridization on permselectivity was therefore the same for morpholino as for DNA probe layers. However, in contrast to the morpholino results, the  $C_d(V_{\text{DC}})$  curve shifted slightly downward. Decrease in capacitance for hybridized DNA probe films was previously attributed to lowering of polarization screening because of volumetric displacement of solvent molecules by DNA targets,<sup>46–48</sup> whose dielectric constant is lower. This explanation also agrees with the present observations. Compared to morpholino films, target hybridization to a DNA probe layer should have little impact on the layer's solvent compatibility because of the good solubility of DNA probes.

The origins of the contrast inversion reported in Figure 3A for morpholino hybridization are now clear. When  $\Delta C_d$  is mea-

(58)  $t_p = (4.9 \times 10^{12} \text{ chains cm}^{-2})(1 \times 10^{-14} \text{ cm}^2 \text{ nm}^{-2})(20 \text{ nt chain}^{-1})(0.53 \text{ nm}^3 \text{ nt}^{-1}) = 0.52 \text{ nm}$ .

(59) A possible explanation for suppression of multivalent phosphate anions, as suggested by the model, is that the dielectric strength inside a probe layer is too low to stabilize multiply ionized phosphate species.

(60) In the model, electrostatic and partitioning penalty energies (eq 5) combine such that a displacement in  $V_{\text{DC}}$  can be compensated through adjustment of the  $\beta_j$  coefficients. This degree of freedom was fixed by assuming  $\beta_{\text{Na}^+} = 0$  for the morpholino monolayer.

(61) Although a three-layer model consisting of an MCP layer, unhybridized probes, and a solution-side layer of more solvated morpholino–DNA hybrids might be more realistic, we continue to use two layers, as this was sufficient to reproduce experiment. Addition of a third, well-solvated and thus high-capacitance layer would, in any case, exert a minor effect, given that smaller capacitances dominate when arranged in series.

(62) Rant, U.; Arinaga, K.; Fujita, S.; Yokoyama, N.; Abstreiter, G.; Tornow, M. *Nano Lett.* **2004**, *4*, 2441–2445.

(63)  $V_{\text{DC}}$  is assumed to not affect the dielectric constant.

sured at a  $V_{DC}$  negative of the  $C_d$  minimum, the unhybridized and uncharged layer is initiated in a cation-rich state. In this scenario, subsequent binding of target strands is accompanied by additional accumulation of cations, rather than expulsion of anions of which there are very few in proximity of the surface. The extra cations are needed to ensure electroneutrality. In this cascade of events, hybridization elevates the local concentration of small ions, ionic screening is enhanced, and thus  $C_d$  increases—leading to positive contrast ( $\Delta C_d > 0$ ). However, as shown by data positive of  $V_{DC} = 0.2$  V in Figure 4A, contrast can be also negative ( $\Delta C_d < 0$ ). Since the  $C_d(V_{DC})$  curve is also translated upward, the decrease in  $C_d$  cannot be attributed to a lowering of the dielectric constant (e.g., from displacement of water molecules by targets). Rather, the explanation is sought in a lowering of the local ionic strength. A diminished ionic strength would imply that hybridization of targets causes a drop in concentration of mobile ions at the surface. This outcome is expected if, as targets bind, electroneutrality is satisfied by expulsion of anions from the surface. Indeed, at sufficiently positive biases the surface concentration of anions will greatly exceed that of cations, making anion expulsion the default mechanism used to satisfy electroneutrality; i.e., the surface ionic strength will drop as targets bind, leading to a negative contrast. The target countercharge, in this case, must then be mostly provided by positive charge on the electrode.

**3.3. Mapping  $\Delta C_d$  to Target Coverage.** The experiments in Figures 3 and 4 helped elucidate physical mechanisms of surface hybridization on morpholino monolayers, but did not provide a quantitative dependence of  $\Delta C_d$  on the extent of hybridization. This dependence was explored in a separate series of measurements using F2-labeled targets, probe coverage of  $5.8 \times 10^{12}$  probes  $\text{cm}^{-2}$ , and six  $V_{DC}$  settings: 0,  $-0.01$ ,  $-0.02$ ,  $-0.03$ ,  $-0.04$ , and  $-0.05$  V. These potentials fall within the diagnostically optimal window in which contrast was strongest and largely potential-independent (Figure 4A).  $C_d$  was determined every 5 min at all six potentials, and immediately following, probe coverage  $S_P$  and target coverage  $S_T$  were measured using cyclic voltammetry (CV). The combined  $C_d$  and CV measurement required 30 s to complete. After subtraction of the  $f_B$  baseline, the six  $\Delta C_d$  values from each time point were averaged and standard deviations calculated. Target and probe coverages were combined into the hybridization conversion  $x$ , defined by  $x = S_T/S_P$ .

Figure 6A plots  $x$  (black points) and  $\Delta C_d$  (red points; error bars are standard deviations) as a function of time, with  $t = 0$  corresponding to addition of complementary TD1 target. The inset shows target and probe coverages calculated from the CV scans shown in Figure 6B. The  $\sim 2\%$  decrease in probe coverage is attributed in part to gradual tag degradation via the ferricinium state.<sup>64,65</sup> In Figure 6B, the peak near 0.24 V is from targets, while that near 0.48 V is from the probes. Surface, as opposed to solution, origins of the target signal were confirmed by noting that the peak current, measured from the baseline, scaled linearly with scan rate  $dV/dt$ .<sup>66</sup> During hybridization, the probe CV peak shifted negatively by about  $-20$  mV and slightly broadened (cf. green and red CV traces in Figure 6B). This shift reflects the creation of a membrane potential<sup>67,68</sup> at the surface from

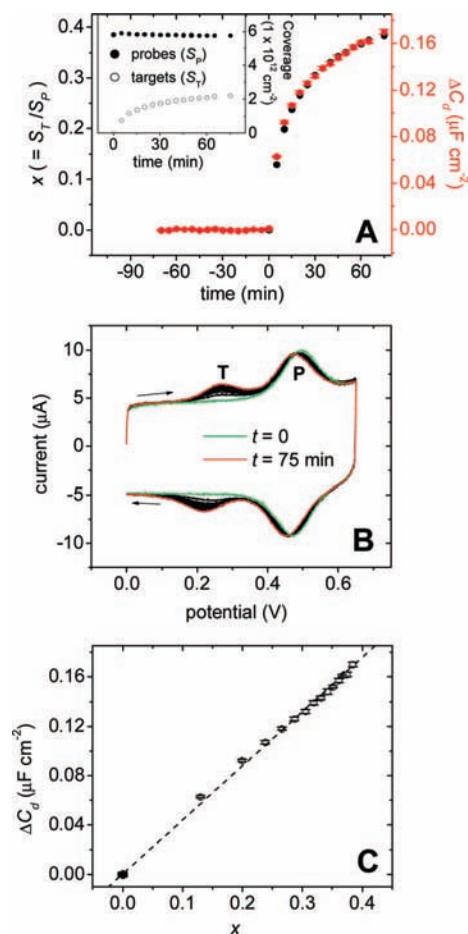


**Figure 6.** (A) Main panel: Time traces of surface conversion  $x = S_T/S_P$  (black points) and of  $\Delta C_d$  signal (red points) for hybridization of TD1 targets to PM1 probes. Plotted  $\Delta C_d$  values are averages of measurements at  $V_{DC}$  of 0,  $-0.01$ ,  $-0.02$ ,  $-0.03$ ,  $-0.04$ , and  $-0.05$  V. Error bars give the standard deviations. Buffer:  $0.2 \text{ mol L}^{-1}$  sodium phosphate, pH 7.0. Inset: Probe (filled points) and target (open points) coverages determined from cyclic voltammetry. (B) Cyclic voltammograms used for calculation of probe and target coverages. First ( $t = 0$ ) and last ( $t = 75$  min) scans are highlighted in green and red, respectively. “T” marks the target peak, and “P” marks the probe peak. (C) Dependence of  $\Delta C_d$  on  $x$ . Dashed line: least-squares linear fit ( $R^2 = 0.9992$ ).

the binding of negatively charged targets, which facilitates oxidation of ferrocene by stabilizing the positively charged ferricinium state. Figure 6C shows that  $\Delta C_d$  and  $x$  were strongly correlated, with a nearly linear relationship between the two quantities.

The label-free limit of quantification,  $l_Q$ , is defined as 10 times  $s_B$ , where  $s_B$  is the standard deviation of the background prior to hybridization (i.e., for  $-70 < t < 0$  min). Performing this calculation on the data in Figure 6A yields  $s_B = 2.2 \times 10^{-10}$  F  $\text{cm}^{-2}$  and  $l_Q = 10s_B = 2.2 \times 10^{-9}$  F  $\text{cm}^{-2}$ . The capacitance units can be converted to more informative units of target coverage by multiplying  $l_Q$  by  $dS_T/d\Delta C_d$ , where  $dS_T/d\Delta C_d = 1.3 \times 10^{19}$  targets  $\text{F}^{-1}$  follows from  $dS_T/d\Delta C_d = S_P (d\Delta C_d/dx)^{-1}$ , with  $d\Delta C_d/dx$  given by the slope of the line in Figure 6C. This yields  $l_Q = 2.9 \times 10^{10}$  targets  $\text{cm}^{-2}$ , representing 0.5% hybridization of the probe layer, or about  $2.5 \text{ pg mm}^{-2}$  of target. This limit is comparable to or exceeds that of surface plasmon

(64) Prins, R.; Korswagen, A. R.; Kortbeek, A. G. T. *J. Organomet. Chem.* **1972**, *39*, 335–344.

(65) Popenoe, D. D.; Deinhammer, R. S.; Porter, M. D. *Langmuir* **1992**, *8*, 2521–2530.

(66) Laviron, E. *J. Electroanal. Chem.* **1974**, *52*, 355–393.

(67) Donnan, F. G. *J. Membr. Sci.* **1995**, *100*, 45–55.

(68) Naegeli, R.; Redepenning, J.; Anson, F. C. *J. Phys. Chem.* **1986**, *90*, 6227–6232.



resonance and quartz crystal microbalance techniques,<sup>69–71</sup> two popular methods for label-free monitoring of surface bioaffinity reactions.

#### 4. Conclusions

Morpholino monolayers on gold can be prepared through direct adaptation of known chemistries for DNA monolayers, in which a thiolate bond serves to anchor morpholino strands through one terminus to the surface, and the rest of the surface is passivated against nonspecific adsorption with a short-chain alkanethiol. Hybridization of morpholino monolayers, which are uncharged, with charged nucleic acid targets alters the dielectric and ionic strength characteristics of the surface environment. Hybridization of target molecules adds negative charge to the probe layer which has to be compensated by changes in local concentrations of small ions, i.e., by accumulation of cations and/or by expulsion of anions. Which adjustment mechanism dominates is tunable by the applied surface potential; e.g., at negative biases, when surface concentration of anions is small, accumulation of cations is the primary response mechanism. At positive potentials, expulsion of anions is dominant. These signatures of hybridization can be monitored through the surface differential capacitance  $C_d$ , where they lead to increases or decreases in  $C_d$  depending on the relative surface populations of cations and anions. Similar phenomena would be expected to arise in electrostatic monitoring of surface hybridization using other uncharged probe molecules, such as PNAs<sup>72–74</sup> or nylon nucleotides.<sup>75,76</sup> The described physical processes are also analogous to those in other systems driven by charge effects, e.g., in metal–oxide–semiconductor structures, where semiconductor dopant sites take the place of immobile target charges

and the phenomena of charge carrier inversion and accumulation correspond to accumulation of anions or cations in the probe layer.

A central motivation for the present study of morpholino surface hybridization is the prospect of label-free DNA or RNA analysis. Based on a 10:1 signal-to-noise criterion,  $C_d$  measurements demonstrated limits of quantification down to  $3 \times 10^{10}$  targets  $\text{cm}^{-2}$ , corresponding to several picograms of material per square millimeter. This performance matches that of other label-free methods, including surface plasmon resonance<sup>69</sup> and quartz crystal microbalance<sup>71</sup> techniques, that could be used for analysis of nucleic acids by surface hybridization. In the case of capacitive transduction, sensitivity is expected to improve at lower ionic strengths, under conditions more dilute than the 0.2 mol  $\text{L}^{-1}$  phosphate buffer used. These and related performance issues will be analyzed separately. If label-free capacitive diagnostics are found promising, they can be adopted to microelectronic biochip platforms, in the spirit of recent efforts to develop fully integrated chip hardware for label-based electrochemical nucleic acid assays.<sup>47,77–79</sup>

**Acknowledgment.** This project was supported by Award No. R33HG003089 from the National Human Genome Research Institute.

**Supporting Information Available:** Description of the synthesis of the FC1 tag; illustration of the conjugation of ferrocene tags to probe and target strands; description of equations and methods used to fit cyclic voltammetry data to extract peak areas; control experiments examining impact of surface potential variation during  $C_d$  measurement; cyclic voltammetry control experiments for nonspecific adsorption of target strands; complete ref 30. This material is available free of charge via the Internet at <http://pubs.acs.org>.

JA810051Q

- (69) Homola, J.; Yee, S. S.; Gauglitz, G. *Sens. Actuators, B* **1999**, *54*, 3–15.  
(70) Su, X. D.; Wu, Y. J.; Knoll, W. *Biosens. Bioelectron.* **2005**, *21*, 719–726.  
(71) Sheikh, S.; Blaszykowski, C.; Thompson, M. *Anal. Lett.* **2008**, *41*, 2525–2538.  
(72) Macanovic, A.; Marquette, C.; Polychronakos, C.; Lawrence, M. F. *Nucleic Acids Res.* **2004**, *32*, e20.  
(73) Uno, T.; Tabata, H.; Kawai, T. *Anal. Chem.* **2007**, *79*, 52–59.  
(74) Aoki, H.; Tao, H. *Analyst* **2007**, *132*, 784–791.  
(75) Zhu, L.; Lukeman, P. S.; Canary, J. W.; Seeman, N. C. *J. Am. Chem. Soc.* **2003**, *125*, 10178–10179.  
(76) Liu, Y.; Wang, R.; Ding, L.; Sha, R.; Lukeman, P. S.; Canary, J. W.; Seeman, N. C. *ChemBioChem* **2008**, *9*, 1641–1648.

- (77) Levine, P. M.; Gong, P.; Levicky, R.; Shepard, K. L. *IEEE J. Solid-State Circuits* **2008**, *43*, 1859–1871.  
(78) Ghindilis, A. L.; Smith, M. W.; Schwarzkopf, K. R.; Roth, K. M.; Peyvan, K.; Munro, S. B.; Lodes, M. J.; Stöver, A. G.; Bernards, K.; Dill, K.; McShea, A. *Biosens. Bioelectron.* **2007**, *22*, 1853–1860.  
(79) Schienle, M.; Paulus, C.; Frey, A.; Hofmann, F.; Holzapfl, B.; Schindler-Bauer, P.; Thewes, R. *IEEE J. Solid-State Circuits* **2004**, *39*, 2438–2445.